Analysis of multifrequency interferometry in a cylindrical plasma

D. J. Kraft, Roger D. Bengtson, and B. N. Breizman
Physics Department, University of Texas at Austin, Austin, Texas 78712
and IFS, University of Texas at Austin, Austin, Texas 78712

D. G. Chavers, C. C. Dobson, and J. E. Jones
Propulsion Research Center, NASA/MSFC, Huntsville, Alabama 35812

V. T. Jacobson
Ad Astra Rocket Company, Houston, Texas 77058

(Received 6 May 2006; presented on 9 May 2006; accepted 7 June 2006; published online 28 September 2006)

A microwave interferometer operating simultaneously at 70, 90, and 110 GHz is used to measure line integrated electron density in a plasma column in the VX-20 experiment. Interferometer beam sizes are a significant part of the plasma radius at some locations. We model the wave propagation through the plasma using a scalar wave approximation with assumptions of a Gaussian beam profile and plasma spatial profile. The phase shifts obtained from this model are compared with standard thin beam calculations and experimental data. © *2006 American Institute of Physics.*
[DOI: 10.1063/1.2222172]

I. INTRODUCTION

Obtaining electron density profiles from microwave interferometry on cylindrical plasmas has been established before for beam sizes small compared to the plasma size not taking refraction into account.[1] Analyzing interferometry data taken simultaneously at 70, 90, and 110 GHz for beam sizes that are a significant part of the plasma radius by using a thin beam assumption without accounting for refraction has led to different electron density estimates for the three frequencies and has motivated this work.

A new approach to model the beam propagation through a cylindrical plasma for beam sizes on the order of the plasma size is presented and compared to experimental results. Both refraction and the finite beam size are accounted for.

II. EXPERIMENTAL SETUP

The microwave interferometer uses a scene beam with a Gaussian transverse profile consisting of three discrete frequencies at 70, 90, and 110 GHz. The full width at half maximum of the beam waist is about 1.8, 1.4, and 1.2 cm at 70, 90, and 110 GHz, respectively. A quadrature configuration provides a means to discriminate between amplitude and phase modulation in the plasma signals.

This interferometer has been used to measure the electron density in the VASIMR VX-20 device.[2,3] The VX-20 experiment employs a helicon discharge in helium which produces a flowing plasma with a high degree of ionization. We discuss measurements at a location where the plasma diameter of ~3 cm is comparable to the beam size.

III. MODELING OF THE WAVE PROPAGATION

We consider a linearly polarized transverse electromagnetic wave traveling perpendicular to the axis of the plasma column as shown in Fig. 1. The plasma frequency is assumed to have a Gaussian profile,

$$\omega_p^2 = \omega_{p0}^2 \exp\left[-\frac{x^2+z^2}{2\rho^2}\right], \tag{1}$$

where $\omega_{p0} \equiv \sqrt{4\pi n_0 e^2/m_e}$, n_0 is the electron density on the axis of the column, and ρ is the plasma radius. We introduce an incident beam at $z=-z_0$ and model the detection of the signal at an observation surface S behind the plasma at $z=z_0$ (Fig. 1).

By combining Maxwell's curl equations, we obtain the wave equation for the electric field E:

$$\nabla^2 E = \frac{4\pi}{c^2}\frac{\partial j}{\partial t} + \frac{1}{c^2}\frac{\partial^2 E}{\partial t^2}, \tag{2}$$

where c is the speed of light, and **j** is the induced electron current. The electric field and the electron current can be represented by

$$E = \mathrm{Re}\{A(x,y,z)\exp[-i\omega_0(t-z/c)]\}, \tag{3}$$

$$j = \mathrm{Re}\{J(x,y,z)\exp[-i\omega_0(t-z/c)]\}, \tag{4}$$

where we assume the plasma frequency ω_p to be small compared to the frequency of the microwave beam, ω_0. E and j are related by the equation of motion for the electrons,

$$\frac{\partial j}{\partial t} = \frac{\omega_p^2}{4\pi}E. \tag{5}$$

Using all of the above in Eq. (2) and assuming furthermore that the second derivative of A with respect to z is negligible leads to a differential equation in A,

$$\frac{\partial^2 A}{\partial x^2} + \frac{\partial^2 A}{\partial y^2} + 2i\frac{\omega_0}{c}\frac{\partial A}{\partial z} = \frac{\omega_p^2}{c^2}A. \tag{6}$$

To solve this equation we use an ansatz of the form

$$A(x,y,z) = R(x,y,z)\exp[i\phi(x,y,z)], \tag{7}$$

where the amplitude $R(x,y,z)$ and the phase $\phi(x,y,z)$ are taken to be real quantities. We then obtain two coupled dif-

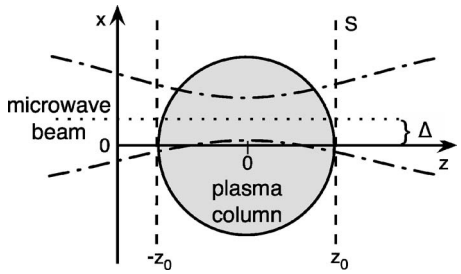

FIG. 1. Schematic representation of a section through the plasma column. We take the beam to be incident on the plasma column at $-z_0$ and to be detected at surface S at z_0. The beam can be offset from the plasma axis by a distance Δ.

ferential equations for $R(x,y,z)$ and $\phi(x,y,z)$, one from each of the real and imaginary parts of Eq. (6):

$$\left[\frac{R_{xx}+R_{yy}}{R}-(\phi_x^2+\phi_y^2)\right]-2\frac{\omega_0}{c}\phi_z=\frac{\omega_p^2}{c^2}, \tag{8}$$

$$[2(R_x\phi_x+R_y\phi_y)+R(\phi_{xx}+\phi_{yy})]+2\frac{\omega_0}{c}R_z=0, \tag{9}$$

where the subscripts x, y, and z in Eqs. (8) and (9) denote spatial derivatives.

The vacuum solution for this set of equations, which represents an incoming Gaussian beam with amplitude R_0 and phase ϕ_0, is given by

$$A_0(x,y,z)=\frac{1}{2\pi(a^2+icz/\omega_0)}\exp\left[-\frac{(x-\Delta)^2+y^2}{2(a^2+icz/\omega_0)}\right]$$
$$\equiv R_0(x,y,z)\exp[i\phi_0(x,y,z)], \tag{10}$$

where a is the beam waist at $z=0$ and Δ is the beam offset in x from the axis of the plasma column (Fig. 1).

To solve Eq. (8) in the presence of a plasma, we treat the quantities in square brackets in Eqs. (8) and (9) perturbatively, which requires $a^4 \gg (cz_0/\omega_0)^2$. Equation (8) is then solved by

$$\phi(x,y,z)=\phi_1(x,y,z)+\delta\phi(x,y,z), \tag{11}$$

where $\delta\phi \ll \phi_1$ and ϕ_1 satisfies the following first order differential equation:

$$-2\frac{\omega_0}{c}\phi_{1z}=\frac{\omega_p^2}{c^2}. \tag{12}$$

We take the boundary condition $\phi_1(x,y,-z_0)=\phi_0(x,y,-z_0)$ into account to obtain

$$\phi_1(x,y,z)=\phi_0(x,y,-z_0)-\frac{1}{2\omega_0 c}\int_{-z_0}^{z}\omega_p^2 dz'. \tag{13}$$

To solve Eq. (8) iteratively for $\delta\phi$, we use the vacuum amplitude R_0 instead of R and disregard the x and y derivatives of the perturbation $\delta\phi$ and the vacuum phase ϕ_0. With Eq. (1) this gives a correction $\delta\phi(x,y,z)$ (Fig. 2) that represents the refraction of the beam due to the density gradient:

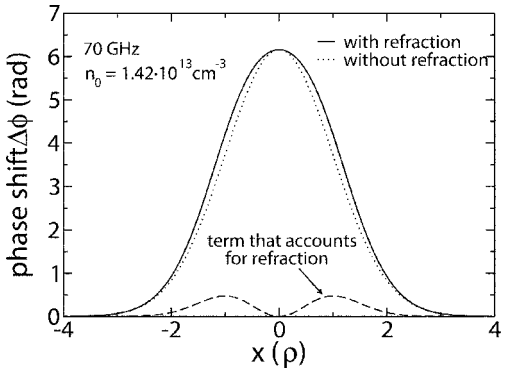

FIG. 2. Phase shift distribution $\Delta\phi=\phi_0-\phi$ behind the plasma ($z=z_0$) plotted as a function of x position (70 GHz, $n_0=1.42\times10^{13}$ cm^{-3}, $\rho=1.5$ cm), both with and without taking refraction by the density gradient into account [Eq. (11)].

$$\delta\phi(x,y,z)=-\frac{1}{8\omega_0^3 c}\int_{-z_0}^{z}\left(\frac{\partial}{\partial x}\int_{-z_0}^{z'}\omega_p^2 dz''\right)^2 dz'$$
$$-\frac{c}{2\omega_0}\int_{-z_0}^{z}\frac{R_{0,xx}+R_{0,yy}}{R_0}dz'. \tag{14}$$

We can safely neglect the second term in Eq. (14), because it enters both the phases of the scene and the reference beam and therefore does not contribute to a phase difference between the two beams.

We chose the location of the detector to be $z_0=2\rho$ in order to pick up $\sim$95.5% of the integral over ω_p^2. This choice of z_0 also fulfills the condition $a^4 \gg (cz/\omega_0)^2$ for all values of z between $-z_0$ and z_0.

Using the phase [Eq. (11)] and the vacuum amplitude $R_0(x,y,-z_0)$ at $z=-z_0$ as the lowest order solution, we find $R(x,y,z)=R_0(x,y,-z_0)+\delta R(x,y,z)$,

$$R(x,y,z)=R_0(x,y,-z_0)-\frac{c}{\omega_0}\left[R_{0x}(x,y,-z_0)\int_{-z_0}^{z}\phi_x dz'\right.$$
$$\left.+\frac{1}{2}R_0(x,y,-z_0)\int_{-z_0}^{z}\phi_{xx}dz'\right]. \tag{15}$$

With Eqs. (11) and (15) the resulting electric field of the scene beam at any position z in the plasma is

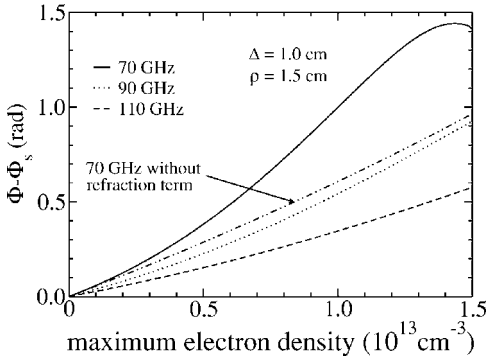

FIG. 3. Absolute difference between the interference phase shifts for our model and those for the standard thin beam model (no refraction) for 70, 90, and 110 GHz at a scan offset $\Delta=1.0$ cm ($\rho=1.5$ cm). Even without the refraction term [Eq. (11)] the phase shift for the finite beam size model is larger than for a thin beam assumption.

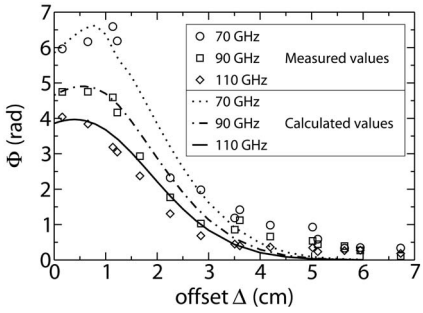

FIG. 4. Comparison of calculated values with experimental data for the profile of the interference phase shift Φ (ρ=1.5 cm, n_0=1.42×10^{13} cm^{-3}).

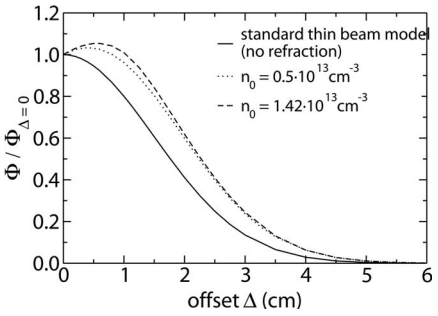

FIG. 5. Interference phase shift normalized to the phase shift at $\Delta=0$ plotted as a function of offset Δ for different maximum densities n_0 at 90 GHz. In addition the normalized interference phase shift for a thin beam model without refraction as a function of offset is plotted.

$$E_{\text{scene}} = \text{Re}\{R(x,y,z)\exp[i\phi - i\omega_0(t - z/c)]\}. \quad (16)$$

To model the detection we superpose E_{scene} with the electric field of a reference beam, $E_{\text{ref}}=\text{Re}[R_0 \exp(i\phi_0 - i\omega_0 t + i\omega_0 z/c)]$. The beams in vacuum are chosen to be in phase at the detection plane S. We account for the quadrature configuration by adding a phase shift $\phi_Q=\pi/2$ to the scene beam. Since the detector is sensitive to the intensity I, we square the resulting electric field E_{total} and integrate over the x-y plane S to obtain the detected signal V,

$$V \sim \int_S I dS \sim \int_S E_{\text{total}}^2 dS = \int_S |E_{\text{scene}} e^{i\phi_Q} + E_{\text{ref}}|^2 dS. \quad (17)$$

Because the detector cannot respond to high frequencies, only the slowly varying parts are of interest and we therefore neglect the high frequency components of the signal V,

$$V \sim \int_S \left\{ \frac{1}{2}[R^2 + R_0(-z_0)^2] + RR_0(-z_0) \times \cos(\phi + \phi_Q - \phi_0) \right\} dS. \quad (18)$$

From Eq. (18) we can define an interference phase shift Φ,

$$\cos\Phi = \frac{\int_S RR_0(-z_0)\cos(\phi + \phi_Q - \phi_0)dS}{\int_S RR_0(-z_0)dS}, \quad (19)$$

which for a thin beam is given by $\cos\Phi_{\text{tb}}=\cos[\phi(\Delta,0,z_0) + \phi_Q - \phi_0]$. If furthermore refraction is neglected, Eq. (19) defines the interference phase shift $\Phi_s = -(1/2\omega_0 c)\int_{-z_0}^{z_0} \omega_p^2 dz'$ for the standard thin beam model in case of densities small compared to the cutoff density [Eq. (11) of Ref. 1, p. 71].

IV. COMPARISON WITH A STANDARD THIN BEAM MODEL AND EXPERIMENTAL DATA

The first term in Eq. (11) represents the phase shift for small densities in the thin beam limit without accounting for refraction. It increases proportionally to the maximum electron density n_0. However, further away from the plasma center the phase contribution from this first term is smaller due to a shorter path length and a smaller electron density. Integrating over the detection area S averages over the different contributions in phase ϕ and amplitude R of each part of the beam and the signals V of the two models differ therefore due to the finite beam size (Fig. 3).

For higher densities the second term in Eq. (11) becomes important because it is proportional to the square of the density gradient. This term accounts for beam refraction. Refraction due to the gradient term always leads to an increase in the interference phase shift as shown in Figs. 2 and 3.

Reducing experimental data using a standard thin beam model does not account for polychromatic differences from the gradient term. Calculations showed that the different beam sizes have relatively small influence on polychromatic differences.

In Fig. 4 we show a comparison of experimentally measured phase shifts for three frequencies (70, 90, and 110 GHz) as a function of offset Δ along with model results for a Gaussian density profile with peak density of 1.42 ×10^{13} cm^{-3} and radius ρ=1.50 cm. We chose these parameters for the model because of visual fit to the data. There may be other profiles that fit the data better. Note that phase shift measurements cannot be easily reduced to profile information because density gradients are a function of both density profile and peak density (Fig. 5).

V. SUMMARY

We have gone beyond the standard interferometry analysis in studying the case where the beam waist is an appreciable fraction of the cylindrical plasma size and beam refraction by density gradients plays an important role. Our model explains the experimentally observed polychromatic differences in the signals.

ACKNOWLEDGMENTS

This research is supported in part by Ad Astra Rocket Company, the German National Academic Foundation, U.S. Department of Energy Grant No. DE-FG02-04-ER 54742, and Johnson Space Center, NASA.

[1] D. Veron, in *Infrared and Millimeter Waves*, edited by K. Button (Academic, New York, 1979), Vol. 2, Chap. 2.
[2] J. P. Squire, F. R. Chang-Diaz, T. W. Glover, V. T. Jacobson, G. E. McCaskill, D. S. Winter, F. W. Baity, M. D. Carter, and R. H. Goulding, Thin Films **506–507**, 579 (2006).
[3] C. C. Dobson, J. E. Jones, and D. G. Chavers, Rev. Sci. Instrum. **75**, 674 (2004).